Emission time and sequence in a $^{58}Ni+^{12}C$ fusionlike source at 34.5 MeV/nucleon

M. Samri,[1,*] L. Gingras,[2,†] F. Grenier,[2] L. Beaulieu,[2,†] J. Gauthier,[2] G. P. Gélinas,[2] Y. Larochelle,[2,‡] J. Moisan,[2] R. Moustabchir,[2] R. Roy,[2] C. St-Pierre,[2] D. Thériault,[2] and A. Vallée[2]

[1]*Laboratoire de Physique Nucléaire et Applications, Université Ibn Tofail, Kénitra, Morocco*

[2]*Laboratoire de Physique Nucléaire, Département de Physique, de Génie physique et d'Optique, Université Laval, Québec, Canada G1K 7P4*

(Received 10 February 2003; published 25 July 2003)

Fusionlike events in $^{58}Ni+^{12}C$ at 34.5 MeV/nucleon are isolated by use of the statistical discriminant analysis method applied to a set of 20 global variables in complete events with at least 90% of the total charge of the system. Two-fragment reduced-velocity correlation functions are measured for the emission of intermediate mass fragments (IMF's) and compared to many-body trajectory calculations. Alpha particle emission sequence has been deduced as a function of excitation energy. At the highest excitations, α particles are emitted simultaneously with IMF's on a time scale of about 200–300 fm/c. In less excited events, they are emitted on a longer time scale. This hybrid deexcitation mechanism, sequential and prompt, is corroborated by comparing the charge of the heaviest and the second heaviest fragments to predictions of GEMINI and SMM simulations.

DOI: 10.1103/PhysRevC.68.014609 PACS number(s): 25.70.Lm, 25.70.Mn, 25.70.Pq

I. INTRODUCTION

New and important facets of nuclear matter have been revealed by studying the formation and deexcitation of nuclei produced in extreme conditions of excitation energy and temperature. One of these is multifragmentation [1,2] for which the most commonly reported theoretical explanation is the entrance of the system into a region of spinodal mechanical instability [3]. Competing deexcitation mechanisms from sequential to simultaneous are also observed in multifragmentation studies. This signature has been previously reported to signal a nuclear liquid-gas phase transition in finite systems [4,5]. Good candidates in such studies are well-defined fused compact single sources formed in inverse-kinematic studies with intermediate-energy heavy ions, which can now be isolated with little contamination from other sources, thanks to exclusive multidetection methods achieved with powerful multidetectors, coupled with new and innovative selection methods [6–14]. Of particular interest in these studies is the time scale associated with fragment and particle emission, which is closely related to the deexcitation mechanisms. This important piece of information is accessible through two-fragment correlation function measurements [15,16] and by particle time sequence model-independent determination techniques [17,18]. This paper is devoted to the study of the $^{58}Ni+^{12}C$system at 34.5-MeV/nucleon incident beam energy and extends previous analysis of this experiment, which considered the quasiprojectile source and the intermediate velocity region formed in this reaction [19–21]. In the present study, we have isolated fused single source events from complete events detected with a large multidetector array, by means of a multivariate statistical method recently applied to select fusionlike events in Ni+Ni [8,9], $^{24}Mg+^{12}C$ [10–12], $^{58}Ni+^{197}Au$ [13] and $^{129}Xe+^{nat}Sn$ [13].

II. EXPERIMENTAL SETUP

The experiment was performed at the tandem accelerator superconducting cyclotron (TASCC) facility at Chalk River by using a ^{58}Ni beam accelerated at 34.5 MeV/nucleon and bombarding a 2.4 mg/cm^2 carbon target. The charged particles produced were detected in the HÉRACLÈS 4π array constituted by 144 detectors set in ten rings concentric to the beam axis and covering polar angles between 3.3° and 140°. The forward four rings (3.3° to 24°) are each made of 16 plastic phoswich detectors with energy detection thresholds of 7.5 (27.5) MeV/nucleon for element identification of $Z=1$ (28) particles. Two rings of 16 CsI(Tl) crystals characterized with low-energy detection thresholds (2 MeV/nucleon for $Z=1,2$ particles) cover polar angles between 24° and 46°. The last four rings (46°–87° and 93°–140°) are constituted by CsI(Tl) crystal detectors set in groups of 12 per ring. The CsI detectors achieve isotopic resolution for $Z=1$ and 2 ions. The energy calibration of the detectors is accurate to about 5%. The events were recorded on an event-by-event basis when at least three detectors were fired.

III. THE DISCRIMINANT ANALYSIS SELECTION METHOD

For the sake of isolating single source events, we have first considered events with a total detected charge equal or greater than 31, which represents 90% of the total charge of the system, and then applied the statistical discriminant analysis (DA) method [9–11]. This technique is used to build a discriminant function, as a linear combination of discriminating variables, that separates occurring groups.

*Corresponding author. Email address: msamri@phy.ulaval.ca

†Present address: Département de Radio-Oncologie, Hôtel-Dieu, 11 cote du Palais, Québec, Canada G1R 2J6.

‡Present address: Joint Institute for Heavy Ion Research, Holifield Radioactive Ion Beam Facility, P. O. Box 2008, Building 6008 MS 6374, O.R.N.L. Oak Ridge, TN 37831-6374.

A. Global variables

In the present experiment, the variables used in the DA method are global characteristics representing the completeness of the event, its form in different coordinate systems, the charge distribution, and the kinematics of the reaction. The variables are the total multiplicity, the charge asymmetry [10], the charge of the heaviest fragment, the relative velocity between particles taken 3×3 (minimum and maximum values) [22,23], the total momentum and charge, the Fox moment of order 2, H_2 [24], the sphericity, coplanarity and aplanarity [25] computed from the kinetic flow tensor [25], the flow angle, the transverse energy, the anisotropy ratio [26], and the total transverse and parallel momenta. The last four quantities are calculated in the center-of-mass and the ellipsoid frames.

B. Simulations and the DA method

A simulation code that tags the nature (one- or two-source) of the event is necessary to customize the DA method. To this purpose, we have used the code DIT [27] to create the entrance ^{58}Ni$+^{12}$C channel and the statistical sequential GEMINI code [28] to deexcite the quasiprojectile (QP), quasitarget (QT), or composite system excited nuclei. The entrance channel model proceeds mainly through stochastic fluctuating transfers of nucleons, energy, and angular momentum between the projectile and target while approaching each other along Coulomb trajectories. The code allows computation of the charge, mass, velocity, excitation energy, and angular momentum of the QP, QT, and the fused system on an event-by-event basis. These observables are used as input to the statistical GEMINI model which describes the subsequent decay of the excited nuclei. The simulated events are filtered through the geometrical and energetic cuts of the experimental array, and events of total charge equal to or greater than 31 are considered to calculate the 20 global variables for each event.

The discriminant function D_g is obtained by using the DA method which gives (in the case of two groups) the best axis that separates these groups. It is given as a linear combination of the discriminating V_i variables, $D_g=\Sigma_{i=1}^{20}a_iV_i$, where the a's are the discriminant coefficients and the V_i's are the global variables previously defined. The top part of Fig. 1 shows the distribution of the discriminant function along with its unfolding into one- and two-source event contributions represented by the dashed (left) and dotted (right) histograms, respectively. The figure shows the good source separation achieved with this method. A cut at $D_g\leqslant-0.2$ keeps 90% of one-source events and removes most of other contributions. It is interesting to quantify these contributions when projecting the global variables obtained with other (different) simulations on the discriminant axis given by the DIT+GEMINI simulations. We have performed such simulations with the standard (cold) version of the SMM model [29,30]. In this code, all fragments are produced simultaneously and are driven apart by Coulomb repulsion. As input to SMM, we have constructed the entrance channel differently than for GEMINI, by using the semiclassical coupled channel-channels code TORINO [31]. This code incorporates the statistical exchange of nucleons between the reaction partners to nuclear structure effects (collective surface modes). The distribution of the discriminant function obtained by projecting the TORINO+SMM global variables on the DIT+GEMINI discriminant axis is given in the middle panel of Fig. 1. Since, in this case, the single- or binary-event type is tagged in the simulations, the distribution is unfolded into one- and two-source events. The figure shows that single-source events correspond to low values of the discriminant function and are separated from binary events. The cut $D_g\leqslant-0.2$ contains less than 20% of binary-type events.

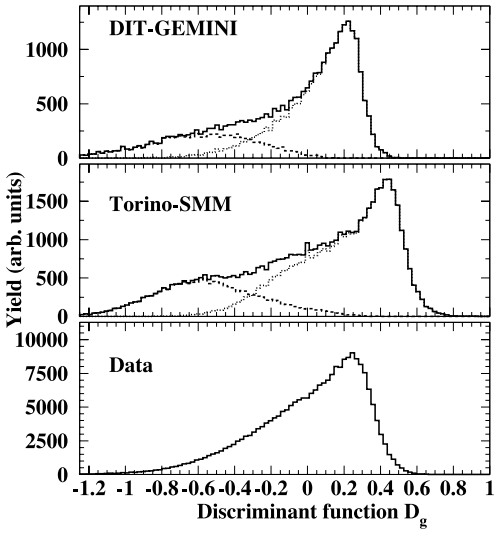

FIG. 1. Distributions of the discriminant function for complete events ($\Sigma Z\geqslant31$) in ^{58}Ni$+^{12}$C reaction for DIT+GEMINI simulations (top), TORINO+SMM simulations (middle), and data (bottom). For simulations, the contribution of one- (two-) sources events are represented by left dashed (right dotted) histograms. For data and SMM simulations, the distributions are obtained by using the discriminant coefficients given by the DIT+GEMINI filtered simulations.

C. Fusionlike event selection

The experimental distribution of the D_g function obtained by projecting the experimental events on the discriminant axis given by the DIT+GEMINI simulations analysis is shown in the lower part of Fig. 1. The distribution covers almost the same range as that obtained by the DIT+GEMINI model or by projecting the TORINO+SMM events on the DIT+GEMINI discriminant axis. Since in the experimental data other emission sources such necklike structures may also be present, the separation valley between one- and two-source events, which is clearly observed in the simulations, is less visible. Yet, the distribution exhibits a disymmetrical shape with the low values of the discriminant function corresponding to one-source events.

In order to verify that the cut $D_g\leqslant-0.2$ isolates effectively these events, we have compared the experimental flow angle distribution for single-source-attributed events isolated with the above cut to the corresponding filtered GEMINI and SMM simulated one-source events. The flow angle is usually used in many works as a sole variable to isolate single-source events [25,14,32,6,33]. It is defined as the angle between the

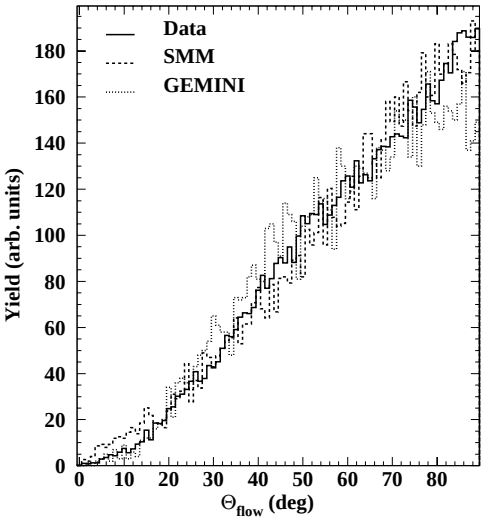

FIG. 2. Flow angle distributions corresponding to fusion events for data, GEMINI and SMM filtered simulations. All distributions are normalized to the same number of counts.

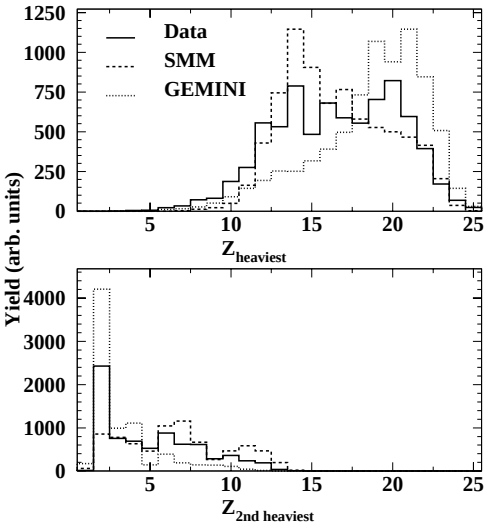

FIG. 3. Distributions of the charge of the heaviest (top) and the second heaviest (bottom) fragments corresponding to fusion events for data, GEMINI, and SMM filtered simulations. All distributions are normalized to the same number of counts.

ellipsoid major axis corresponding to the highest eigenvalue of the kinetic energy tensor (preferred direction of emitted matter) and the beam axis. Fused events, which have lost the memory of their entrance channel, should be isotropic, and the associated flow angle distribution should be peaking at $\theta_{flow}=90°$ as shown in Fig. 2 for filtered GEMINI and SMM simulated single-source events, and also in Refs. [33,34].

The experimental flow angle distribution for experimental fused events (isolated with the condition $D_g \leqslant -0.2$) exhibits a shape closely resembling that of the filtered simulated events. Although the flow angle is used among the discriminating variables to build the discriminant function, its contribution to this function is only about 7%. It is worthwhile to note that a sharp cut in the flow angle distribution greater than 60° would reject a good proportion of single-source events, and thus would degrade the properties of the fused source. The flow angle selection method may be an adequate source selector for heavy systems characterized with high multiplicities and large fragments in which the kinetic energy tensor is well defined. For relatively small systems such as that under study, characterized with low multiplicities, the multivariate method, which uses a large number of variables, may be better adapted than the flow angle.

IV. EXPERIMENTAL RESULTS AND DISCUSSION

A. Charge distributions of the two heavy fragments

As a first and simple observable to probe the deexcitation mechanisms, we consider the charges of the heaviest and the second heaviest fragments which are static properties characterizing the topology of the event. In sequential decay occurring at low excitations, the heaviest fragment will be a heavy residue produced after a sequence of light particle emissions. At higher excitations, intermediate mass fragments are produced and the charge of the heaviest fragment will be lower than in sequential decay. This is well illustrated (and reproduced) in Fig. 3 representing the charge of the two heaviest fragments in these two limiting situations given by the filtered GEMINI (sequential) and SMM (prompt) simulations. The experimental distribution for the heaviest fragment, given in the top panel of the figure, has a large width and covers the range of both simulations. The same trend is also observed in the bottom part of the figure for the second heaviest fragment. This shows that data can be described as a mixture of sequential and prompt emissions.

B. Two-fragment reduced-velocity correlation functions

This qualitative picture may be further investigated by constructing correlation functions between intermediate mass fragments (IMF's) [15,16] which provide information about the time scale involved in the decay process. These are often built with the reduced velocity between pairs of IMF's defined by $v_{red}=v_{rel}/\sqrt{Z_1+Z_2}$ [15], where v_{rel} is the relative velocity between charges Z_1 and Z_2. The correlation function is given by

$$1+R(v_{red})=C\frac{N_{corr}(v_{red})}{N_{uncorr}(v_{red})}. \quad (1)$$

$N_{corr}(v_{red})$ is the reduced-velocity distribution for pairs of IMF's coming from the same (correlated) event, and $N_{uncorr}(v_{red})$ is the background distribution with uncorrelated pairs of IMF's each one coming from a different event.

In order to extract the fragment emission time, the experimental correlation function is constructed and compared to the simulated ones performed by the many-body Coulomb trajectory code of Glasmacher *et al.* [35–38]. This code assumes fragments to be emitted sequentially from the surface of a spherical source with emission times having the probability distribution $P(t)\approx e^{-t/\tau}$ with τ being the source emission time. After each emission, recoil velocity and mass conservation of the source are taken into account. The charge,

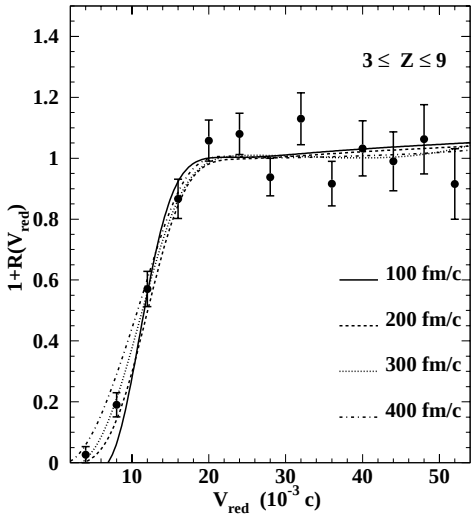

FIG. 4. Two-IMF correlation functions, integrated over all $3 \leqslant Z \leqslant 9$ fragment pairs originating from one-source-attributed events. The curves represent calculated correlation functions of a Coulomb trajectory calculation for different emission times.

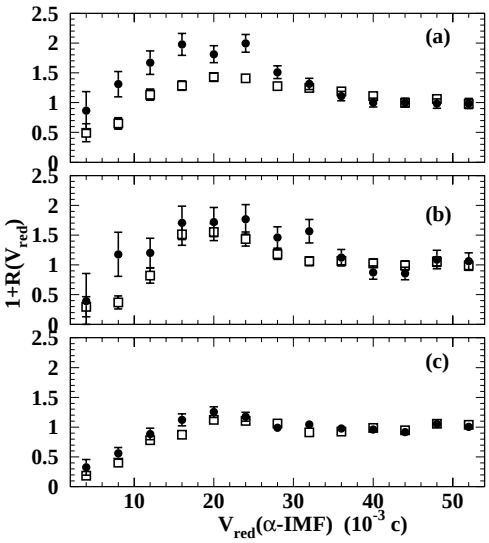

FIG. 5. The experimental α-IMF correlation function with a relative velocity selection for three increasing bins of excitation energy 3.4, 4.5, and 5.5 MeV/nucleon represented in figure parts (a), (b), and (c) respectively. Solid symbols refer to the case where α particles are slower than IMF's in the single-source frame. Square symbols refer to the opposite situation.

mass and energy of fragments and the residue charge are randomly sampled from the experimental distributions.

The experimental and simulated correlation functions with different emission times are displayed in Fig. 4. The χ^2 values are 0.867, 0.861, 0.859, and 0.883 for increasing times respectively. The best fits to the experimental function yielding minimum χ^2 value are obtained with the simulated functions performed with emission times of 200 -300 fm/c. It is well known that a relationship exists between emission times and excitation energy [39,37,19]. In the multifragmentation events considered to build the correlation functions characterized with two and more IMF's, the mean excitation energy is 4.8 MeV/nucleon. The excitation energy is constructed from the charged decay products of the fusionlike nucleus, on an event-by-event basis, by summing up the total kinetic energy and the channel Q value and correcting the computed value for unobserved neutrons with the method used in Ref. [10]. The emission time determined here is comparable to that reported for the QP [19] in the same reaction under study presently, and at the same excitation energy. Such an emission time is considered to be short [15] and is usually associated with a prompt multifragmentation decay.

C. Alpha particle emission order

The time scale for α particle emission, relative to that of IMF's, is deduced with the help of the particle-chronology technique. This technique is based on the analysis of the speed difference (velocity module difference) of a pair of charged particles [17]. Authors of Ref. [18] have shown, in a theoretical study, that it can be extended to all kinds of nonidentical particles. Recently, the time sequence for light (p,d,t,α) particles has been deduced via this method [40–42] in central collisions. The principle of the method is to compare the correlation function constructed with a pair of particles 1 and 2 when particle 1 is faster than 2 in the source frame to the correlation function constructed in the other situation. If a time delay in the emission of the particles exists, the Coulomb suppression effect would be enhanced for pairs of particles for which the average distance is smaller. This would be the case if the first emitted particle is slower than the second one. We have applied this method to probe the time sequence between α particles and IMF's. Since α particles are produced in different processes (multifragmentation, evaporation), the chronology of emission may be only an average of these processes. To avoid this, events are divided into three classes of increasing excitation energy.

Figure 5 shows the experimental α-IMF correlation function when α particles are slower than IMF's and in the opposite situation for the three classes of events with mean excitation energies of 3.4, 4.5, and 5.5 MeV/nucleon. For less-excited events, represented in part (a) of the figure, the Coulomb suppression is more visible in the case of α particles faster than IMF's. It can be deduced that α particles are emitted on a longer time scale than IMF's. For highly excited events given in part (c) of the figure, the Coulomb suppression is the same in both α-IMF relative velocity selections, indicating that α particles are emitted on average at the same time as IMF's. Medium-excited events, represented in part (b) of the figure are intermediate between these two cases. This same trend is also observed when classifying the events with the number of IMF's as a parameter. The Coulomb suppression is the same in both α-IMF relative velocity for events characterized with three IMF's or more. On the contrary, for one-IMF-type events, the Coulomb suppression is more pronounced in the case of α particles faster than IMF's. These observations are consistent with a picture in which α particles are emitted on a longer time scale in low-excited evaporationlike events than in highly excited multifragmentation ones. This suggested time scale and its correlation with

excitation energy are consistent with the above-cited relationship of emission times as a function of excitation energies [39,37,19]. The general picture that can be drawn from this study is that of a hierarchy of deexcitation mechanisms, evaporation and multifragmentation, following each other with increasing excitation energy. Events with two and more IMF's represent about 12% of the total fused events. So, despite indications of simultaneous decay, supported by the determined time scale and by the distribution of the charge of the two heaviest fragments, the data can be generally described by a sequential binary decay picture.

V. SUMMARY AND CONCLUSION

To summarize, we have isolated a fused single source by considering complete events to which we have applied the statistical DA method. This selection technique has been validated by making use of other simulated events whose source origin is tagged, and by comparing the experimental flow angle distribution to one-source distributions obtained with two different simulations. Two-fragment reduced-velocity correlation functions for the emission of intermediate mass fragments were constructed and compared to many-body trajectory calculations. The results indicate an emission time of about $200-300$ fm/c. The α particle chronology emission with respect to IMF emission has been determined for different events as a function of excitation energy and with the number of emitted IMF's as a parameter. Alpha particles are found to be emitted promptly with IMF's in multifragmentation events, and on a longer time scale in evaporation data. These results are consistent with the general picture of decreasing times with excitation energy and corroborates the qualitative comparison of the charge of the event-2 heaviest fragments to sequential and simultaneous simulations. A non-negligible part of the single-source data can be viewed as a prompt decay process. Yet, the sequential binary decay seems to dominate.

ACKNOWLEDGMENTS

We would like to thank our collaborators from Chalk River Laboratories. This work was supported in part by the Natural Sciences and Engineering Research Council of Canada and the Fonds pour la Formation de Chercheurs et l'Aide à la Recherche du Québec. The authors are grateful to Dr. R. J. Charity, Dr. A. Botvina, Dr. T. Glassmacher, and Dr. Tassan-Got for supplying the codes used in this work. M.S. acknowledges the kind hospitality of the Laboratoire de Physique Nucléaire, Département de Physique, de Génie physique et d'Optique, Université Laval.

[1] C.K. Gelbke and D.H. Boal, Prog. Part. Nucl. Phys. **19**, 3 (1987).
[2] L.G. Moretto and G.J. Wozniak, Annu. Rev. Nucl. Part. Sci. **43**, 397 (1993).
[3] J. D. Gunton and M. Droz, *Introduction to the Theory of Metastable and Unstable States*, Lecture Notes in Physics, 183 (Springer-Verlag, Berlin, 1983).
[4] H. Jaquaman *et al.*, Phys. Rev. C **27**, 2782 (1983).
[5] F. Gulminelli and Ph. Chomaz, Phys. Rev. Lett. **82**, 1402 (1999).
[6] L. Beaulieu *et al.*, Phys. Rev. Lett. **77**, 462 (1996).
[7] J. Péter *et al.*, Nucl. Phys. **A593**, 95 (1995).
[8] A. M. Maskay-Wallez, Ph.D. thesis, Université Claude Bernard I, Lyon I, France, LYCEN T 9969 (1999).
[9] P. Désesquelles *et al.*, Phys. Rev. C **62**, 024614 (2000).
[10] M. Samri *et al.*, Nucl. Phys. **A700**, 42 (2002).
[11] M. Samri *et al.*, Phys. Rev. C **65**, 061603(R) (2002).
[12] F. Grenier, Masters thesis, Université Laval, Canada, QC 3.5 UL 2002 G827 (2002).
[13] N. Bellaize *et al.*, Nucl. Phys. **A709**, 367 (2002).
[14] J.D. Frankland *et al.*, Nucl. Phys. **A689**, 905 (2001).
[15] Y.D. Kim *et al.*, Phys. Rev. C **45**, 338 (1992); **45**, 387 (1992).
[16] D.R. Bowman *et al.*, Phys. Rev. Lett. **70**, 3534 (1993).
[17] C.J. Gelderloos *et al.*, Nucl. Instrum. Methods Phys. Res. A **349**, 618 (1994).
[18] R. Lednicky *et al.*, Phys. Lett. B **373**, 30 (1996).
[19] Zhi-Yong He *et al.*, Phys. Rev. C **65**, 014606 (2001).
[20] L. Gingras *et al.*, Phys. Rev. C **65**, 061604(R) (2002).
[21] A. Chernomoretz *et al.*, Phys. Rev. C **65**, 054613(R) (2002).
[22] O. Lopez *et al.*, Phys. Lett. B **315**, 34 (1993).
[23] R. Bougault *et al.*, Nucl. Phys. **A488**, 255c (1988).
[24] C.G. Fox and S. Wolfram, Phys. Rev. Lett. **41**, 1581 (1978).
[25] J. Cugnon and D. L'Hote, Nucl. Phys. **A397**, 519 (1983).
[26] H. Strobele *et al.*, Phys. Rev. C **27**, 1349 (1983).
[27] L. Tassan-Got and C. Stéphan, Nucl. Phys. **A524**, 121 (1991).
[28] R.J. Charity *et al.*, Nucl. Phys. **A476**, 516 (1988).
[29] A.S. Botvina *et al.*, Nucl. Phys. **A507**, 649 (1990).
[30] J.P. Bondorf *et al.*, Phys. Rep. **257**, 133 (1995).
[31] C.H. Dasso and G. Pollarolo, Comput. Phys. Commun. **50**, 341 (1988).
[32] J.F. Lecolley *et al.*, Phys. Lett. B **325**, 317 (1994).
[33] Y. Larochelle *et al.*, Phys. Rev. C **62**, 051602(R) (2000).
[34] Y. Larochelle *et al.*, Phys. Rev. C **55**, 1869 (1997).
[35] T. Glasmacher *et al.*, Phys. Rev. C **50**, 952 (1994).
[36] R. Popescu *et al.*, Phys. Rev. C **58**, 270 (1998).
[37] L. Beaulieu *et al.*, Phys. Rev. Lett. **84**, 5971 (2000).
[38] Zhi-Yong He *et al.*, Phys. Rev. C **63**, 011601(R) (2001).
[39] D. Durand *et al.*, Phys. Lett. B **345**, 397 (1995).
[40] R. Kotte *et al.*, Eur. Phys. J. A **6**, 277 (1999).
[41] D. Gourio *et al.*, Eur. Phys. J. A **7**, 245 (2000).
[42] L. Gingras, Ph.D. thesis, Université Laval, Canada, QC 3.5 UL 2002 G492, 2002.